Nanodiamond Catalysts

DOI: 10.1002/anie.201002869

Surface Chemistry and Catalytic Reactivity of a Nanodiamond in the Steam-Free Dehydrogenation of Ethylbenzene**

Jian Zhang, Dang Sheng Su, Raoul Blume, Robert Schlögl, Rui Wang, Xiangguang Yang, and Andreja Gajović*

The finite resources of fossil fuels and the worsening global climate have stimulated tremendous interest in searching for energy-saving and nonpolluting catalysts that can be used in conventional reactions. Styrene, an important raw material for polymer synthesis, is mostly produced by direct dehydrogenation (DH) of ethylbenzene (EB). Unfortunately, carbonaceous species inevitably deposit on the surface of multiply promoted Fe catalysts and cause a sharp loss of activity. Hence, excess steam must be recycled to remove the resulting "coke", and thus much energy is wasted. Given what is known about the mode of operation of Fe catalysts, no breakthrough is to be expected from a conventional system.[1] Therefore, some alternative routes have been proposed such as side-chain alkylation of toluene with methanol[2] and oxidative dehydrogenation (ODH) with oxygen,[3] but they exhibit either insufficient selectivity or risks in handling flammable mixtures. We report here that carbon chemistry leads to a great improvement in a traditional catalytic reaction, by allowing steam-free dehydrogenation of ethylbenzene.

Nanocrystalline diamond has triggered many theoretical and practical studies over the past few decades. Currently, it is used as polishing agent, coating material, polymer additive, and lubricant, to name just a few of its applications.[4] Synthetic nanodiamonds have an average size ranging from 4 to 8 nm.[5] Their large surface-to-volume ratio endows them with higher surface reactivity than other forms of carbon, so that they have many other potential applications, including biological composites, catalyst supports, sensors for bacteria, and electrochemical coatings.[6] The nanodiamond we studied here is commercially produced by detonation synthesis. After refluxing with oxidizing acids, the content of sp^3 carbon atoms is $(93.3 \pm 1.3)\,\%$, as determined by fitting the first part of the electron energy-loss near-edge structure (ELNES) of the carbon K edge with three Gaussians centered at around 285, 287, and 292 eV.[7] The sp^2 carbon atoms on the surface are functionalized by carboxyl, anhydride, hydroxyl, ketonic carbonyl, and lactone groups.[4] Among them, unsaturated ketone-/diketone-type carbonyl groups (C=O) have substantial electron density at the oxygen atom, and thus can serve as Lewis bases to activate saturated hydrocarbons.

The structural and surface properties of our nanodiamond were investigated by high-resolution (HR) transmission electron microscopy (TEM), electron energy-loss spectroscopy (EELS), in situ diffuse-reflectance infrared Fourier transform (DRIFT), and synchrotron-excited X-ray Photoelectron Spectroscopy (XPS). The images in Figure 1a,b clearly evidence the existence of a core–shell structure. The diamond nanoparticle at the core is about (5 ± 2) nm in diameter, and a thin carbon shell forms a curved and defective surface. The shell gives a very weak π^* peak characteristic of sp^2-hybridized carbon, while the sp^3-hybridized diamond only allows the transitions of 1s electrons to the unoccupied σ^* states in the EELS spectrum (see below). Such an sp^2–sp^3 hybrid structure was predicted by several computational and experimental investigations on so-called bucky diamond.[8]

Both in situ DRIFT and XPS tests reveal the dynamics of surface and functionalization of the nanodiamond on heating. Figure 1c illustrates the key vibrational features of the nanodiamond surface.[9] Physically adsorbed water is negligible after pretreatment of the sample at 120 °C overnight. With increasing temperature, the band near 3465 cm^{-1} decreases to a great extent due to thermal removal of O–H bonds in hydroxyl groups and hydrogen bonds, probably arising from dehydration of neighboring ones. Decreasing bands at 3109, 3053, 2970, and 1405 cm^{-1} indicate gradual loss of hydrocarbon bonds such as C–H. The C=O stretching band centered at 1795 cm^{-1} remained unchanged in shape and position with increasing temperature up to 450 °C. We attribute it mainly to ketonic/diketonic carbonyl groups on account of its superior stability at elevated temperatures.[10] The bands of ether-like C–O bonds between 1097 and 1319 cm^{-1} decrease in intensity while the feature is retained.

[*] Prof. J. Zhang, Prof. D. S. Su, Dr. R. Wang
Shenyang National Laboratory for Materials Science,
Institute of Metal Research, Chinese Academy of Sciences
72 Wenhua Road, Shenyang 110016 (China)
Prof. J. Zhang, Prof. D. S. Su, R. Blume, Prof. R. Schlögl
Department of Inorganic Chemistry,
Fritz Haber Institute of the Max Planck Society
Faradayweg 4–6, Berlin 14195 (Germany)
Fax: (+49) 30-8413-4401
E-mail: dangsheng@fhi-berlin.mpg.de
Prof. X. G. Yang
State Key Laboratory of Rare Earth Resource Utilization,
Changchun Institute of Applied Chemistry (China)
Dr. A. Gajović
Molecular Physics Laboratory, Rudjer Boskovic Institute
Zagreb (Croatia)

[**] We thank the European Union (CANAPE project), the Max Planck Society (EnerChem project), and the Croatian Ministry of Science Education and Sport (098-0982904-2898) for financial support. J. Zhang thanks NSFC (No. 50921004) and the Institute of Metal Research (O9NBA111A1) for basic funding. We gratefully acknowledge BESSY for XPS tests, J. Kröhnert, D. Wang, Profs. F. Jentoft, F. S. Xiao, M. Muhler, C. Hébert, and P. McGuiness for helpful discussions and assistance.

Supporting information for this article is available on the WWW under http://dx.doi.org/10.1002/anie.201002869.

View this journal online at wileyonlinelibrary.com

© 2010 Wiley-VCH Verlag GmbH & Co. KGaA, Weinheim

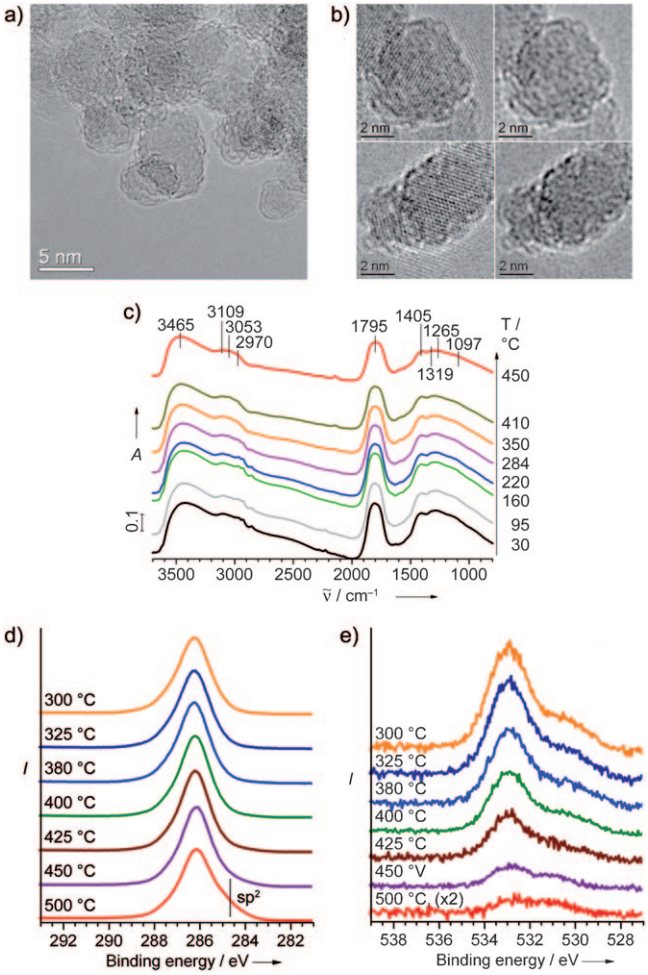

Figure 1. Characterization of fresh nanodiamond. a) HRTEM image of a typical area. b) HRTEM images (left) and inverse fast Fourier transform images after filtering crystalline diamond (right). c) In situ DRIFT spectra at 30–450 °C in vacuum. d) In situ C(1s) and e) O(1s) XPS spectra up to 500 °C in vacuum, respectively.

Figure 1 d,e shows XP spectra of nanodiamond at various temperatures. The coexistence of an sp^3-hybridized diamond core and an sp^2-hybridized graphitic shell is confirmed by peaks at 286.2 and 284.7 eV in C(1s) spectra, respectively.[11] Slight graphitization of the diamond phase is clearly observed at 450 °C. Two prevailing oxygen species were identified in the O(1s) spectra (Figure 1 e), namely, unsaturated C=O and saturated C–O components at 530.9 and 532.9 eV, respectively. As the temperature was increased from 350 to 450 °C, the concentration of O_{C-O} decreased from 73.1 to 65.0 %, while that of $O_{C=O}$ increased from 17.4 to 35.0 %, that is, $O_{C=O}$ species have superior thermal stability. At the same time, the total amount of oxygen decreased from 5.2 to 1.3 %, and this was attributed to thermal desorption of the less-stable functional groups.

The catalytic activity of nanodiamond was evaluated at 550 °C under atmospheric pressure by using diluted ethylbenzene as reactant. Dry dehydrogenation conditions were chosen to allow direct comparison with the performance of a typical K-promoted Fe_2O_3 catalyst. The activity of the K–Fe catalyst dropped rapidly from 20.2 to 9.2 % over 2 h and then stayed at about 7.1 %. Nanodiamond shows 2.8 times the steady-state activity of the K–Fe catalyst. Figure S1 (Supporting Information) shows heavy coke formation on the used K–Fe catalyst, which is believed to be the major reason for its low activity by blocking most of the active surface. Another interesting finding is that the high initial activity of nanodiamond can be fully restored by flowing air through the catalyst at 400 °C. As shown in Figure S2 (Supporting Information), similar profiles are observed after five successive regeneration runs lasting for a total of 120 h. Moreover, the used nanodiamond displays remarkable stability over a long period of time. The yield and selectivity are greater than 20.5 and 97.3 %, respectively (Figure 2 a), and suggest a bright future for industrial applications.

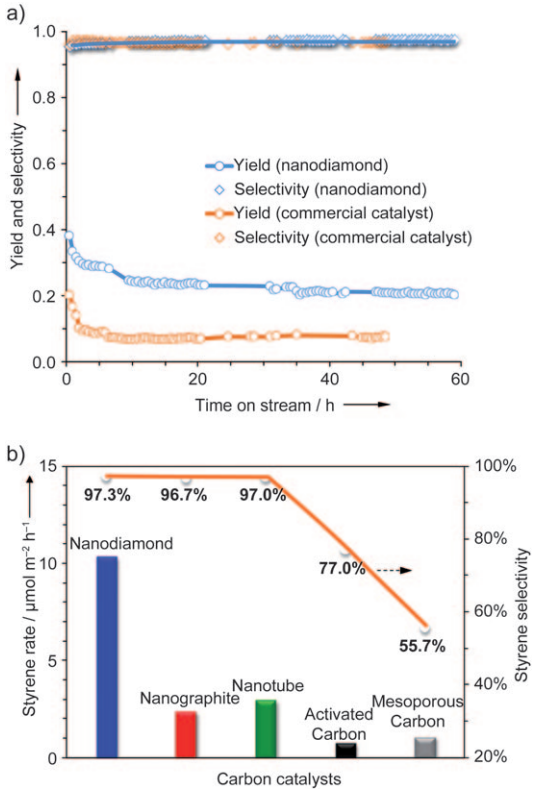

Figure 2. Ethylbenzene (EB) dehydrogenation activity of nanodiamond. a) Long-term performance with activity of commercial Fe_2O_3 catalyst for comparison; data from sixth cycle in Figure S2 (Supporting Information). b) Steady-state activities of various carbons. Reaction conditions: 0.05 g, 550 °C, 2.8 % EB in helium, 10 mL min^{-1}.

Nanodiamond is much more active and selective than other carbon materials, including carbon nanotubes, nanographite, activated carbon, and mesoporous carbon. Figure 2 b illustrates the specific reaction rates as the amount of styrene produced per square meter of surface per hour. Nanodiamond displays a value as high as 10.3 μmol m^{-2} h^{-1}, up to 14 times those of other samples. All nanocarbons provide higher selectivity of around 97.0 % than mesoporous carbon and activated carbon (55.7–77.0 %). The inferior activity is mainly related to their short- or long-range disorder

 © 2010 Wiley-VCH Verlag GmbH & Co. KGaA, Weinheim

with mixtures of sp^2- and sp^3-hybridized carbon giving a variety of surface groups and defects that allow α- or β-scission of ethylbenzene into benzene and toluene.

Perfect graphene is terminated at its basal plane by a sheet of sp^2 carbon atoms in hexagonal cells. The edges of the defective sites are mostly saturated with O and/or H atoms. Bending of defective graphene seems to be a consequence of its interaction with certain substrates,[12,13] such as nanodiamond and nanotubes. First-principles calculations have revealed that the defect sites in bent graphene units are active for water disproportion,[14] which is part of the reaction sequence during regeneration of the active sites. The spatial arrangement of spherical nanodiamond provides good access for the reactants, and thus favors interaction with the surrounding hexagonal cell as a π-conjugated system. The curvature of the graphene layer is expected to provide superior activity,[15] because of partial delocalization of the π-electron density. Another reason for the high activity of nanodiamond in the endothermic reaction may be the extremely high thermal conductance of the sp^3 diamond at the core, which could improve heat-transfer efficiency close to the active sites on the surface.

Our proposed mode of operation is based on a simple chemical concept. Ketonic C=O groups, as the electron donor, activate the alkane fragment of ethylbenzene.[3] Styrene is produced and hydroxyl groups (C–OH) remain as intermediates. The reaction cycle is closed by the thermal decomposition of C–OH to C=O and molecular hydrogen, which is thermodynamically favorable at high temperatures. The rigidity of the covalent bonding network and the unique electronic structure of graphene allow the catalyst to reversibly store electrons with little geometric disturbance, and thereby provide considerable activity. This might help to desorb the styrene product and enable H_2 formation from hydroxyl groups (Figure S3, Supporting Information). Besides thermal cleavage from the graphene substrate, deactivation of the C=O active sites can be further induced by hydrogen passivation. Exposing the deactivated sample to air can remove the adsorbed H atoms by reaction with O_2 and restore the activity (Figure S2, Supporting Information).

We performed in situ ambient-pressure XPS and DRIFT experiments to monitor the chemical state at the working surface. Figure 3a shows O(1s) XP spectra of nanodiamond in vacuum and in 0.25 mbar ethylbenzene. Especially at 450 °C, the fraction of $O_{C=O}$ decreased from 35.0 to 15.4 %, while that of O_{C-O} increased from 65.0 to 75.0 %, as a consequence of reduction of C=O to C–OH by the hydrocarbon. We estimate that the reduced activity agrees well with the consumption of $O_{C=O}$,[16] and indicate a relationship between ketonic C=O species and the dehydrogenation reaction.

Infrared spectra recorded at 450 °C are shown in Figure 3b as a function of the time on stream of diluted ethylbenzene. Table S1 (Supporting Information) summarizes the band assignment. The changes for the reactant are observed in three regions. The first is located in the range 3000–3500 cm^{-1} corresponding to C–H and O–H stretching vibrations. Two groups of bands at 3066/3030/2975 cm^{-1} and 1491/1449 cm^{-1} are assigned to the stretching of C–H and skeletal C–C bonds in ethylbenzene, respectively.[17,18] The

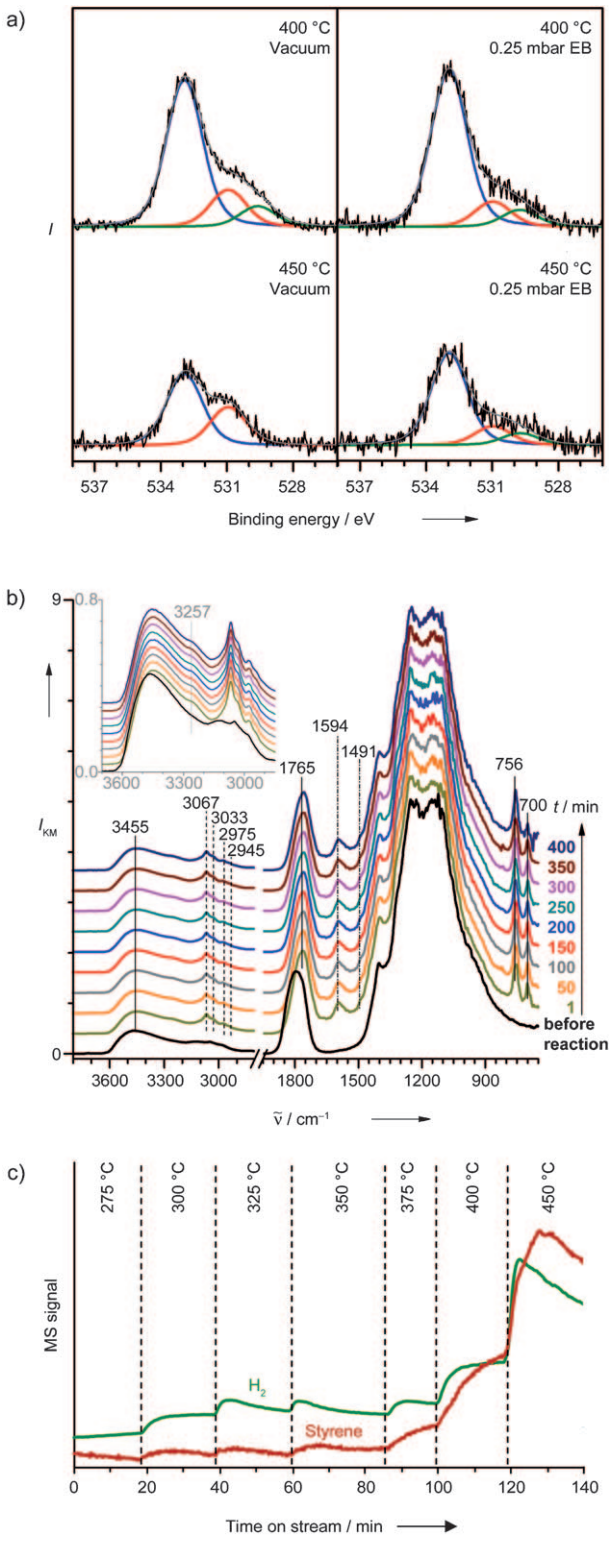

Figure 3. Characterization of nanodiamond catalysts. a) In situ O(1s) XPS spectra in vacuum and 0.25 mbar EB vapor (529.6 eV is assigned to the inert pyridine oxide component). b) In situ DRIFT spectra in a flow of diluted EB at 450 °C. c) H_2 and styrene formation during the in situ XPS measurement in (a).

fact that all aromatic spectral bands remained almost unchanged indicates negligible interaction between the

 © 2010 Wiley-VCH Verlag GmbH & Co. KGaA, Weinheim

benzene nuclei and the surface. Contact of ethylbenzene with the surface gives rise to intense O–H bands near 3470 cm^{-1}, indicating formation of hydroxyl-like intermediates. The second region, at mid-range frequencies, exhibits the C=O modes ($\nu_{C=O}$, 1700–1800 cm^{-1}) of ketonic carbonyl groups on the catalyst, and of C–C (ν_{C-C}, 1440–1600 cm^{-1}) in the aromatic rings of the reactant. A significant redshift from 1790 to 1765 cm^{-1} indicates activation of C=O bonds. Their gradual consumption correlates well with the reduced activity (Figure S4, Supporting Information). We thus conclude a pivotal role of $O_{C=O}$ species in the dehydrogenation activity.

We then consider the possible details of the reaction turnover. The band located at 700 cm^{-1} reflects the out-of-plane bending mode of all mono-substituted benzenes, while the neighboring band at 756 cm^{-1} is sensitive to the nature of the substituent. The latter cannot be assigned to either reactants or products in the dehydrogenation reaction, for example, ethylbenzene (740 cm^{-1}), styrene (775 cm^{-1}), and toluene (725 cm^{-1}). It could correspond to a substituted aromatic alcohol such as 1-phenylethanol (698/760 cm^{-1}) or 1-phenyl-1,2-ethanediol (700/754 cm^{-1}).[19] The whole reaction is then suggested to proceed via the transient state, in which α- or β-H in ethylbenzene chemically bonds with ketonic O atoms, while the benzene nucleus is mostly skewed to the surface. This interpretation is indeed corroborated by the facts above. First, activation of ketonic C=O moieties is most probably realized as acetone condensation, in which addition of C–H usually causes a shift of the C=O band to low frequencies.[20] Adsorption of H_2 is also reported to shift a C=O band from 1757 to 1746 cm^{-1}.[10] Furthermore, all vibrations of the benzene nucleus of ethylbenzene are unaffected and similar to those in the gas phase. The reduction of ketonic C=O components enhances the intensity of hydroxyl bands.

The nanodiamond surface remained clean even after a long period of time (Figure S5, Supporting Information). The EELS spectrum of the used sample contains all the features of a fresh sample, except for the increased intensity of the π excitation. This is due to slight graphitization during the prolonged reaction period, as evidenced by the C(1s) XPS spectra in Figure 1c. The absence of coke formation was confirmed by temperature-programmed oxidation (TPO), which showed no combustion at low temperature (Figure S6, Supporting Information). However, a noticeable change to the surface is caused by hydrogen. Figure 3b shows a stepwise increase of desorbed hydrogen with temperature, as monitored online by mass spectrometry during the in situ XPS tests. At each temperature, the amount of H_2 being formed drops at the beginning of the reaction and then approaches a steady state. Hydrogen passivation was elucidated by checking the combustibility of fresh and used samples by TPO. As seen in Figure S7 (Supporting Information), the used material released around twice the amount of H_2O, which suggests enhanced coverage with H after the reaction. The decreased number of exposed active sites would lead to a drop in the initial activity. Regeneration of some passivated sites ($C-OH \rightarrow C=O + 0.5\,H_2$) may be kinetically slow and thus limits the overall rate. The fresh and used carbon catalysts were also tested by the Raman method. Although the small-size nanodiamond only displayed spectra with extremely low signal-to-noise ratio, the presence of coke can be ruled out according to the almost unchanged D/G band ratios of other carbons (Figure S8, Supporting Information).

In summary, we have described the application of nanodiamond as a novel catalyst for direct dehydrogenation of ethylbenzene under steam-free conditions. The unique sp^2–sp^3 hybrid structure results in different behavior to other carbons, with superior activity and stability and freedom from coke formation. We have also demonstrated how applying the "nano" concept to carbon gives a major advance in catalysis with great potential in the chemical industry. The simplicity of the defective graphene makes it a promising model in complicated reaction scenarios, which are impossible to unravel with metal oxide systems due to the inherent chemical complexity, including terminal and bridging lattice oxygen, various forms of polyvalent metals, and side reactions. We believe there is still a lot of room for more novel catalysts, and a clear understanding of the mechanism is still required.

Experimental Section

Nanodiamond and nanographite ribbon were bought from Beijing Grish Hitech Co. (China). The nanodiamond was synthesized by the detonation method followed by acid washing, and its high-temperature graphitization produced nanographite. Multiwalled carbon nanotubes (Tsinghua University, China) were washed with concentrated HNO_3 to remove residual metal. Activated carbon (1163 $m^2 g^{-1}$; COMBICAT Research Center, University of Malaya, Malaysia) was made from palm kernel shells. Mesoporous carbon (843 $m^2 g^{-1}$) was synthesized from SBA-15 powder as template according to procedures in the literature.[21] A commercial catalyst (9% K_2O–86% Fe_2O_3, Mo and Al as promoters; ST1613-1, BASF, Germany) was also tested for activity.

Dehydrogenation of ethylbenzene was carried out at 550 °C in a quartz microreactor with 0.05 g of catalyst. The system was heated to reaction temperature and kept for 10 min in He. The reactant (2.8% EB, total flow rate 10 mL min^{-1}, He as balance, residual O_2 ca. 26 ppm[22]) was then fed to the reactor from a saturator kept at 40 °C. Hydrocarbons were analyzed by a Varian CP-3800 gas chromatograph equipped with an FID detector. The conversion (X_{EB}) and styrene selectivity (Sel) were calculated according to Equations (1) and (2).

$$X_{EB} = 1 - F C_{EB,outlet} / F_0 C_{EB,inlet} \quad (1)$$

$$Sel_{ST} = C_{ST,outlet} / (C_{ST,outlet} + C_{BZ,outlet} + C_{TOL,outlet}) \quad (2)$$

F and F_0 are the flow rates of the outlet and inlet, respectively, and C_{EB}, C_{ST}, C_{BZ}, and C_{TOL} the concentrations of ethylbenzene, styrene, benzene, and toluene, respectively. The resulting carbon balance varies in the range of (100 ± 4)% in all reactions. The specific rate is expressed as amount of styrene produced per square meter of carbon surface per hour (μmol $m^{-2} h^{-1}$). After completion of the reaction, the sample was purged with high-purity He for 20 min and then cooled to room temperature. A fresh sample was heated in He for 2 h at 550 °C and characterized ex situ for comparison.

TEM and EELS were performed with a Philips CM200 FEG microscope operating at 200 kV, equipped with Gatan Tridiem imaging filter and EDAX energy-dispersive X-ray (EDX) spectrometer. Scanning electron microscopy (SEM) was done with a Hitachi S4800 microscope operating at 15 kV with EDAX detector. Temperature-programmed oxidation/thermogravimetric (TPO/TG) analysis was performed on a Netzsch-STA 449 F3 instrument with alumina

 © 2010 Wiley-VCH Verlag GmbH & Co. KGaA, Weinheim

crucibles and an AVI Omnistar mass spectrometer. Samples were heated in a flow of 20 % O_2 in He to 1000 °C with a ramp of 5 °C min^{-1}. DRIFT spectra were recorded at a resolution of 4 cm^{-1} on Bruker IFS-66 FTIR spectrometer equipped with The Selector accessory (Graseby Specac), an environmental chamber and a D315M MCT detector. The temperature was gradually increased in a flow of 1.3 % EB. Synchrotron-excited XPS analysis was performed at Berliner Elektronenspeicherring, Gesellschaft für Synchrotronstrahlung m.b.H. (BESSY, beamline U49/2-PGM1). The binding energy was calibrated with respect to the Fermi edge of Cu and Au. Ethylbenzene was frozen with liquid N_2 and then heated several times to remove dissolved air. The sample was heated to the target temperature (200–450 °C) under ultrahigh vacuum by laser from the rear.[23]

Received: May 12, 2010
Published online: October 1, 2010

Keywords: carbon · dehydrogenation · heterogeneous catalysis · nanoparticles

[1] A. Schüle, U. Nieken, O. Shekhah, W. Ranke, R. Schlögl, G. Kolios, *Phys. Chem. Chem. Phys.* **2007**, *9*, 3619.
[2] a) J. M. Serra, A. Corma, D. Farrusseng, L. Baumes, C. Mirodatos, C. Flego, C. Perego, *Catal. Today* **2003**, *81*, 425; b) S. K. Ritter, *Chem. Eng. News* **2007**, *85*, 46.
[3] a) D. S. Su, N. Maksimova, J. J. Delgado, N. Keller, G. Mestl, M. J. Ledoux, R. Schlögl, *Catal. Today* **2005**, *102–103*, 110; b) J. Zhang, D. S. Su, A. Zhang, D. Wang, R. Schlögl, C. Hébert, *Angew. Chem.* **2007**, *119*, 7460; *Angew. Chem. Int. Ed.* **2007**, *46*, 7319; c) J. Zhang, X. Wang, Q. Su, L. Zhi, A. Thomas, X. Feng, D. S. Su, R. Schlögl, K. Müllen, *J. Am. Chem. Soc.* **2009**, *131*, 11296; d) L. F. Wang, J. Zhang, D. S. Su, Y. Y. Ji, X. J. Cao, F. S. Xiao, *Chem. Mater.* **2007**, *19*, 2894; e) D. S. Su, N. I. Maksimova, G. Mestl, V. L. Kuznetsov, V. Keller, R. Schlögl, N. Keller, *Carbon* **2007**, *45*, 2145; f) J. Zhang, X. Liu, R. Blume, A. Zhang, R. Schlögl, D. S. Su, *Science* **2008**, *322*, 73; g) J. A. Maciá-Agulló, D. Cazorla-Amorós, A. linares-Solano, U. Wild, D. S. Su, R. Schlögl, *Catal. Today* **2005**, *102–103*, 248.
[4] S. Osswald, G. Yushin, V. Mochalin, S. O. Kucheyev, Y. Gogotsi, *J. Am. Chem. Soc.* **2006**, *128*, 11635.
[5] M. Ozawa, M. Inaguma, M. Takahashi, F. Kataoka, A. Krüger, E. Ōsawa, *Adv. Mater.* **2007**, *19*, 1201.
[6] M. Baidakova, A. Vul′, *J. Phys. D Appl. Phys.* **2007**, *40*, 6300.
[7] A. C. Ferrari, A. Libassi, B. K. Tanner, V. Stolojan, J. Yuan, L. M. Brown, S. E. Rodil, B. Kleinsorge, J. Robertson, *Phys. Rev. B* **2000**, *62*, 11089.
[8] a) A. De Vita, G. Galli, A. Canning, R. Car, *Nature* **1996**, *379*, 523; b) A. S. Barnard, S. P. Russo, I. K. Snook, *Phys. Rev. B* **2003**, *68*, 073406; c) A. Krueger, *J. Mater. Chem.* **2008**, *18*, 1485.
[9] T. Ando, K. Yamamoto, M. Ishii, M. Kamo, Y. Sato, *J. Chem. Soc. Faraday Trans.* **1993**, *89*, 3635.
[10] A. Dandekar, R. T. K. Baker, M. A. Vannice, *Carbon* **1998**, *36*, 1821.
[11] Yu. V. Butenko, S. Krishnamurthy, A. K. Chakraborty, V. L. Kuznetsov, V. R. Dhanak, M. R. C. Hunt, L. Šiller, *Phys. Rev. B* **2005**, *71*, 075420.
[12] M. Ishigami, J. H. Chen, W. G. Cullen, M. S. Fuhrer, E. D. Williams, *Nano Lett.* **2007**, *7*, 1643.
[13] D. D. Quinn, J. P. Wilber, C. B. Clemons, G. W. Young, A. Buldum, *Int. J. Nonlinear Mech.* **2007**, *42*, 681.
[14] M. K. Kostov, E. E. Santiso, A. M. George, K. E. Gubbins, M. B. Nardelli, *Phys. Rev. Lett.* **2005**, *95*, 136105.
[15] J. M. Carlsson, M. Scheffler, *Phys. Rev. Lett.* **2006**, *96*, 046806.
[16] The XP spectrum at 450 °C shows the reduced $O_{C=O}$ fraction to be (35 % − 15.4 %)/35 % = 56 %. As shown in Figure S3 (Supporting Information), the activity in a differential reactor at 475 °C decreased from 5.2 to 2.1 mmol$_{styrene}$ g$_{cat}^{-1}$ h^{-1}, which yields a similar extent of 60 %.
[17] W. P. Addiego, C. A. Estrada, D. W. Goodman, M. P. Rosynek, *J. Catal.* **1994**, *146*, 407.
[18] A. E. Klingbeil, J. B. Jeffries, R. K. Hanson, *J. Quant. Spectrosc. Radiat. Transfer* **2007**, *107*, 407.
[19] NIST/EPA Gas-Phase Infrared Database, NIST Standard Reference Database Number 69, http://webbook.nist.gov/chemistry/.
[20] M. I. Zaki, M. A. Hasan, L. Pasupulety, *Langmuir* **2001**, *17*, 768.
[21] L. F. Wang, S. Lin, K. F. Lin, C. Y. Yin, D. S. Liang, Y. Di, P. W. Fan, D. Z. Jiang, F.-S. Xiao, *Microporous Mesoporous Mater.* **2005**, *85*, 136.
[22] If 100 % conversion of 26 ppm O_2 is assumed, the rate of ODH is 2.7×10^{-2} mmol g^{-1} h^{-1}, which is two orders lower than the measured overall rate, that is, 3.2–4.9 mmol g^{-1} h^{-1}. The DH reaction is thus prevalent with a share greater than 99.3 %.
[23] M. Salmeron, R. Schlögl, *Surf. Sci. Rep.* **2008**, *63*, 169.

 © 2010 Wiley-VCH Verlag GmbH & Co. KGaA, Weinheim